Ab Initio Phase Diagram of Gold in Extreme Conditions

P. Richard,[1,2] A. Castellano,[3] R. Béjaud,[1,2] L. Baguet,[1,2] J. Bouchet,[4] G. Geneste,[1,2] and F. Bottin[1,2]
[1]*CEA, DAM, DIF, F-91297 Arpajon, France*
[2]*Université Paris-Saclay, CEA, Laboratoires des Matériaux en Conditions Extrêmes, 91680 Bruyères-le-Châtel, France*
[3]*NanoMat/Q-Mat/CESAM and European Theoretical Spectroscopy Facility, Université de Liège (B5), B-4000 Liège, Belgium*
[4]*CEA, DES, IRESNE, DEC F-13108 Saint-Paul-Lez-Durance, France*

(Received 19 May 2023; revised 3 August 2023; accepted 12 October 2023; published 15 November 2023)

A phase diagram of gold is proposed in the [0; 1000] GPa and [0; 10 000] K ranges of pressure and temperature, respectively, topologically modified with respect to previous predictions. Using finite-temperature *ab initio* simulations and nonequilibirum thermodynamic integration, both accelerated by machine learning, we evaluate the Gibbs free energies of three solid phases previously proposed. At room temperature, the face-centered cubic (fcc) phase is stable up to ∼500 GPa whereas the body-centered cubic (bcc) phase only appears above 1 TPa. At higher temperature, we do not highlight any fcc-bcc transition line between 200 and 400 GPa, in agreement with ramp-compressed experiments. The present results only disclose a bcc domain around 140–235 GPa and 6000–8000 K, consistent with the triple point recently found in shock experiments. We demonstrate that this re-stabilization of the bcc phase at high temperature is due to anharmonic effects.

DOI: 10.1103/PhysRevLett.131.206101

The emergence of fourth-generation x-ray sources based on synchrotron radiation or free-electron lasers [1], combined with the continuous development of diamond anvil cell (DAC) devices [2] and laser facilities, paves the way to enlarge the description of matter in extreme conditions. For that purpose, gold is a prototypical material used in nuclear fusion for the hohlraum [3] and also employed as a pressure calibration standard for DAC experiments [4–6]. Its face-centered cubic (fcc) structure is stable in a wide range of pressure and temperature [7,8], with a well-established equation of state (EoS) at room temperature from 0 to 131 GPa [9–11], and temperature effects have also been investigated [12–16]. However, recent compression experiments with double DAC [17,18], toroidal DAC [19], laser-driven shock [20–22], or quasi-isentropic ramp [23–25] reach regions of the phase diagram hitherto unexplored at the theoretical level, making it essential to build a phase diagram of Au under a wider *pT* range and to resolve the discrepancies observed by the experimental and theoretical results.

Using DAC devices, Dubrovinsky *et al.* [26] obtained a fcc phase stable at low pressure, then a hexagonal close packed (hcp) phase between 240 and 300 GPa on heated and cooled samples (see Fig. 1). Subsequent room temperature experiments [17–19] did not reveal any hcp or body centered cubic (bcc) phase up to at least 600 and ∼1000 GPa, respectively. This result is confirmed by recent *in situ* diffraction measurements on ramp-compressed Au samples [23,25] at higher temperature (∼2000 K around 600 GPa). Note that Coppari *et al.* [25] no longer observe any phase transition toward a bcc at 377 GPa on ramp compression, as previously proposed [24]. At very high temperature (above 4000 K), some laser-driven shock experiments disclosed a liquid-bcc coexistence between 220 and 302 GPa [22] or a liquid-fcc-bcc triple point around 220 GPa [21] along Hugoniot.

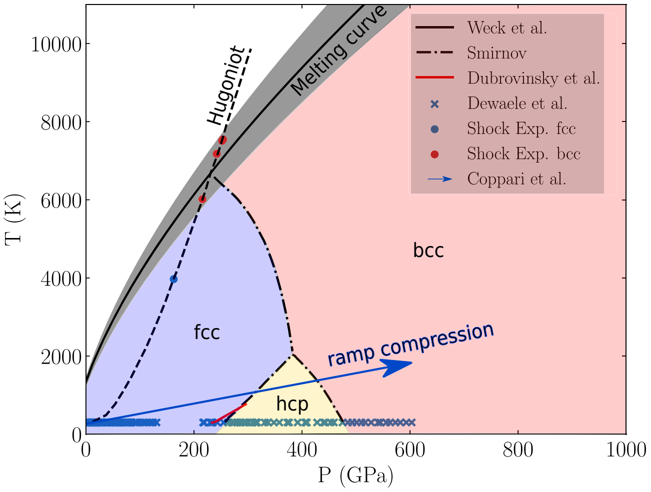

FIG. 1. Sketch of the gold phase diagram with the melting curve (black solid line) of Weck *et al.* [27] extrapolated from 110 GPa to 1 TPa using their Simon-Glatzel equation, room temperature DAC data [19] (blue crosses), fcc-hcp transition observed using heated and cooled samples [26] (red solid line), ramp compression [23,25] (blue solid line), shock experiments [21,22] (blue and red filled circles), and the transition lines from the theoretical work of Smirnov [28] (black dashed and dotted lines).

Early 0 K *ab initio* studies [7,29,30] of Au predicted a fcc-hcp phase transition pressure between 151 and 410 GPa, depending on the exchange and correlation functional used in density functional theory (DFT) simulations, and a bcc phase above 400 GPa [30]. If considering the double hcp (dhcp) phase in the calculations, a fcc-dhcp transition was found around 250 GPa [26,31]. More recently, theoretical works [8,28] investigated the stability of various stacking sequences of the hexagonal structure, the fcc (ABC stacking sequence of the closed packed layers), hcp (AB), dhcp (ABAC), and abcacb (ABCACB) phases, in conjunction with the bcc phase, and found diverging results concerning 0 K transition pressures. If Ishikawa *et al.* [8] found a fcc-abcacb-dhcp-hcp-bcc phase order with transition pressures at 390, 540, 830, and 930 GPa, respectively, Smirnov [28] found sharply lower fcc-hcp and hcp-bcc transition pressures at 225 and 475 GPa, respectively. Above 2000 K, using the quasiharmonic (QH) approximation, Smirnov predicts the disappearance of the hcp phase and the emergence of a fcc-bcc line transition up to the triple point found experimentally, whereas Liu *et al.* [31] highlight the permanency of the 0 K transition sequence.

In this Letter, we use an explicit temperature framework to predict an *ab initio* phase diagram for Au based on Gibbs free energy calculations in a wide pT range. This phase diagram reproduces the vast majority of experimental observations. The Gibbs free energies of three crystallographic phases (fcc, hcp, and bcc) are computed with a high level of accuracy by performing finite temperature *ab initio* simulations and nonequilibrium thermodynamic integration both accelerated using machine learning, in particular, in some ranges of pressure and temperature where these data cannot be deduced from ground state calculations using the QH approximation. We obtain (i) a fcc-abcacb-dhcp-hcp phase sequence transition at 0 K in line with some theoretical results, (ii) no fcc-bcc line transition between 200 and 400 GPa at room and middle temperatures, as revealed by DAC and quasi-isentropic compressions, and (iii) a bcc bubble domain at high temperature between 140 and 235 GPa, consistent with the fcc-bcc-liquid triple point seen in shock experiments.

To determine stability domains of solids and liquid phases, the Gibbs free energy

$$G(p,T) = F(V,T) + pV \tag{1}$$

of each phase has to be computed for a given pressure p, volume V, and temperature T and compared to each other. However, the free energy $F(V,T)$ is not directly accessible from molecular dynamics or Monte Carlo simulations in their standard use. In this work, we employ two methods to evaluate $F(V,T)$ for solid phases as described below. The first procedure is to split the total free energy in three terms as

$$F(V,T) = U_0(V) + F_{\mathrm{el}}(V,T_{\mathrm{e}}) + F_{\mathrm{vib}}(V,T_{\mathrm{i}}), \tag{2}$$

with $U_0(V)$ the cold curve, F_{el} and F_{vib} the electronic and vibrational free energies, respectively, with electronic T_{e} and ionic T_{i} temperatures set equal. The total pressure is then the sum of the 0 K and thermal (electronic, potential, and kinetic) parts, such as $p = p_0 + p_{\mathrm{th}}^{\mathrm{el}} + p_{\mathrm{th}}^{\mathrm{pot}} + p_{\mathrm{th}}^{\mathrm{kin}}$. Using first-principles calculations, one can directly compute $U_0 + F_{\mathrm{el}}$ for any volume and (electronic) temperature. The vibrational contribution F_{vib} is evaluated using either a harmonic formulation based on 0 K phonon spectrum from density functional perturbation theory (DFPT) or anharmonic phonon spectrum from finite temperature simulations. For the latter, we use the temperature dependent effective potential (TDEP) [32–34] method which incorporates the explicit effects in an effective way. This approach has given good results, even for strongly anharmonic solids [57–63], but requires *ab initio* molecular dynamic (AIMD) simulations for each phase, temperature, and volume, leading to a computational time cost out of reach in the present study.

In order to circumvent this issue, we use the machine learning accelerated canonical sampling (MLACS) procedure [34,64] which speeds up the sampling of the equilibrium canonical distribution by training iteratively a machine learning interatomic potential (MLIP), for a given solid phase and thermodynamic state. This method requires a sample of approximately 100 representative configurations to converge locally optimal MLIP. At each step of the MLACS procedure, 20 configurations are computed using *ab initio* calculations on which the MLIP is updated. The self-consistent loop is stopped when the finite temperature phonon frequencies differ within 0.2 meV between two steps. An acceleration of one or two orders of magnitude is obtained compared to AIMD, while maintaining an *ab initio* accuracy over phonon frequencies and free energies (≤ 1 meV/atom).

The second method employed to compute free energy of solid phases in this work is the thermodynamic integration method [65] in a nonequilibrium version [34,66] (NETI) as recently implemented in LAMMPS [67]. This method has the advantage to fully take into account anharmonic effects and to be usable for both solids [67] and liquids [68], unlike TDEP. However, NETI also requires very long AIMD trajectories, preventing its use in an extensive way. In this work, rather than performing NETI between the reference and *ab initio* systems directly, we implement a method [69] proceeding in two steps: we carry out NETI between a known reference potential and the MLIP, then add the free energy difference between the MLIP and *ab initio* distributions as a second-order cumulant obtained with free-energy perturbation. This contribution is generally low since the MLIP gives an equilibrium canonical distribution almost equal to the *ab initio* one, and is negligible in the present case. We applied this procedure recently [64] for classical systems and demonstrated that this one (i) does not require any additional *ab initio* calculations other than those carried out to build the MLIP (~ 100) and (ii) can be applied with success without loosing precision $(\leq 1$ meV/atom$)$. The current work is its first application in the framework of *ab initio* simulations. Compared to a recent and similar approach [69], present MLACS + NETI implementation, based on an equilibrium canonical distribution and a locally optimal MLIP, leads to an order of magnitude better accuracy.

The DFT calculations are performed using the projector augmented wave (PAW) method [70,71] implemented in ABINIT [72,73] and the local density approximation (LDA) for the exchange-correlation functional [74]. The PAW sphere radius of the atomic data [75] equals to 2.5 Å, with 6s and 5d electrons in the valence which leads to a plane-wave cutoff energy equal to 15 Ha. Ground state structural optimizations are performed on the unit cell of the five (fcc, abcacb, dhcp, hcp, and bcc) crystallographic phases for pressures between 0 and 1 TPa using a $(24 \times 24 \times 24)$ **k**-point mesh. In this framework, the equilibrium volume, bulk modulus, and the 0 K equation of state of the fcc phase agree very well with room temperature experiments [10,19,34]. The finite temperature *ab initio* calculations are performed using MLACS in the NVT canonical ensemble and are carried out on supercells with 108 (fcc), 128 (bcc), and 128 (hcp) atoms. A $(2 \times 2 \times 2)$ **k**-point mesh is found to be sufficient to achieve convergence on thermal properties with an error lower than 10 GPa on transition pressures [34]. Then, NETI simulations are performed with the local MLIP on larger supercells with 6912 atoms for fcc and 8192 atoms for bcc and hcp phases, with a switching time of 500 and 25 ps equilibration time.

The enthalpy differences (at 0 K) with respect to the fcc phase (see the top left panel in Fig. 2) highlight a fcc-abcacb-dhcp-hcp-bcc transition sequence. These results are consistent with the data of Ishikawa *et al.* [8] and, to a lesser extent, with those obtained by Dubrovinsky *et al.* [26], which are both produced using a PAW-LDA framework similar to the present one. On the other hand, at odds with Söderlind *et al.* [30] and Smirnov [28], the bcc phase does not appear before 1 TPa in the present calculations, which has also been reported by several theoretical studies [7,8,26,29]. The dhcp and abcacb phases, almost degenerated with hcp one and not seen experimentally, will be no longer considered thereafter. At room temperature (see Fig. 2), NETI and TDEP free-energy differences agree perfectly, validating the present MLACS + NETI strategy. At higher temperature, when anharmonic effects become larger, some discrepancies appear and the calculation of TDEP effective harmonic free energies appears more limited. At $T = 300$ K, the hcp phase stabilizes between 500 and 600 GPa, whereas the fcc phase is stable up to 603 GPa in experiments [19]. This slight disagreement could have two origins. First, various approximations in present calculations (exchange and correlation functional, PAW atomic data) can alter the *ab initio* accuracy and lead to strong shifts $(\sim 100$ GPa$)$ in transition pressures [34]. Second, the energetic proximity of the fcc and hexagonal phases can induce some metastabilities which would affect experiments [26] as discussed by Sharma *et al.* [76] who highlight the role of stacking fault formation on high pressure structural transformations in shocked noble metals. Nevertheless, the stability domain of the hcp phase decreases with temperature (see the bottom panels in Fig. 2), which is consistent with the result predicted by Smirnov [28] using the QH approximation. The fcc-bcc transition pressure, being almost unaffected by temperature, leads to an increase of the fcc domain toward higher pressure at high temperature.

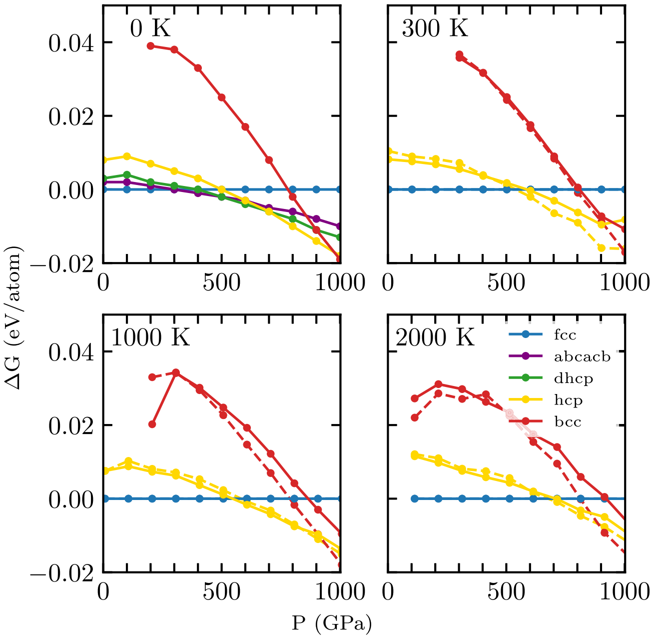

FIG. 2. Gibbs free-energy differences (eV/atom) between the bcc, abcacb, dhcp, hcp, and fcc phases at 0, 300, 1000, and 2000 K. NETI (solid lines) and TDEP (dashed lines). Free energies are computed independently, which leads to slightly rough curves. Melted and dynamically unstable points are removed, whereas the bcc phase at (1000 K, 200 GPa) is at the verge of a dynamical instability (see Fig. 5).

The NETI method having been validated at low temperature (see Fig. 2), we then apply it at higher temperatures (see Fig. 3 and Ref. [34]) where anharmonic effects are larger. The hcp domain, which reduces at higher temperature, disappears above 6000 K. The increase of the fcc domain is consistent with ramp-compressed [23,25] experiments which only see a fcc crystallographic phase at very high pressure and intermediate temperature. In addition to the bcc domain standing above 1 TPa, the present calculations suggest a restabilization of the bcc phase around 140–235 GPa and 6000–8000 K. For several pT points just

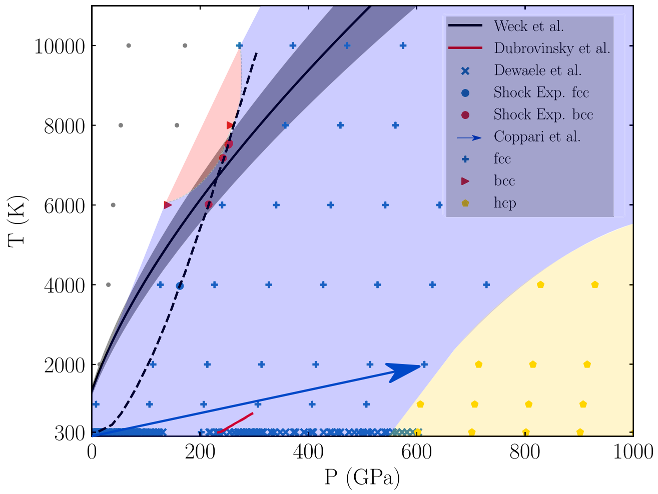

FIG. 3. Au phase diagram obtained using MLACS simulations and Gibbs free-energy NETI calculations. Several experimental results [19,21,25–27] (see Fig. 1) are also plotted.

above the experimental fcc melting line extrapolated from 110 to 1000 GPa, the Gibbs free energies of the bcc phase are lower than the fcc ones. This result, in agreement with the observation of a bcc phase in shock experiments [21,22], implies that a bcc melting curve would stand above the fcc one beyond 140 GPa.

This restabilization of the bcc phase at low pressure, between 140 and 235 GPa, and close to the melting temperature is remarkable. At low temperature, as demonstrated by the imaginary frequencies of the phonon spectra computed with DFPT at 0 K and TDEP at 300 K (see Fig. 4), the bcc structure is indeed dynamically (and mechanically [34]) unstable at low pressure and stabilizes at higher pressure. Consequently, the QH approximation cannot apply to evaluate the thermodynamic stability of the bcc phase at low pressure [34].

In Fig. 5 we present the phonon spectrum of the bcc phase computed using TDEP between 300 and 10 000 K along the $V = 77.69\ \mathrm{Bohr}^3/\mathrm{at}$ isochore (around 200 GPa). We can notice two explicit temperature effects, which would not occur in QH approximation since all phonon spectra would be equal all along the isochore. First, the soft modes around Γ disappear with temperature, leading to a dynamical stabilization of the bcc phase at high temperature. Second, the decreasing of the bcc phonon spectrum (which does not arise for the fcc one [34]) provides a significant anharmonic contribution to the Gibbs free energy (~ -100 meV/atom at 8000 K) and a thermodynamic stabilization of the bcc phase at high temperature. These two explicit temperature effects are responsible for the emergence of a bcc phase at high temperature, as also shown for other materials [32,58,62,69,77,78] (Ti, Zr, Hf, U...). However, to our knowledge, it is the first time that a bcc bubble domain arises at low pressure, disconnected from a high pressure bcc domain, without any transition line from low to high temperature.

In this work, we have investigated the equilibrium phase diagram of gold up to 1000 GPa and 10 000 K by means of MLACS and NETI simulations, both accelerated by machine learning. A phase sequence transition (fcc-abcacb-dhcp-hcp-bcc) is obtained at 0 K. At room

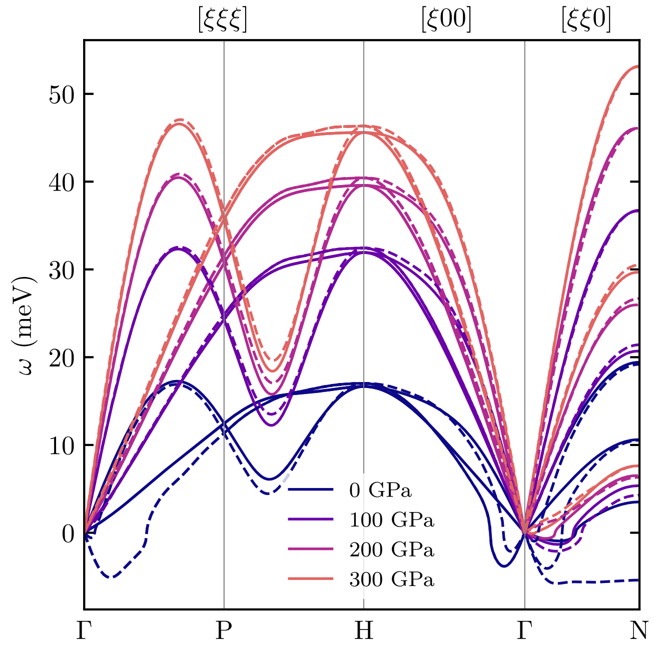

FIG. 4. Phonon spectrum of bcc-Au at 0, 100, 200, and 300 GPa computed with MLACS-TDEP at 300 K (solid lines) and with DFPT at 0 K (dashed lines).

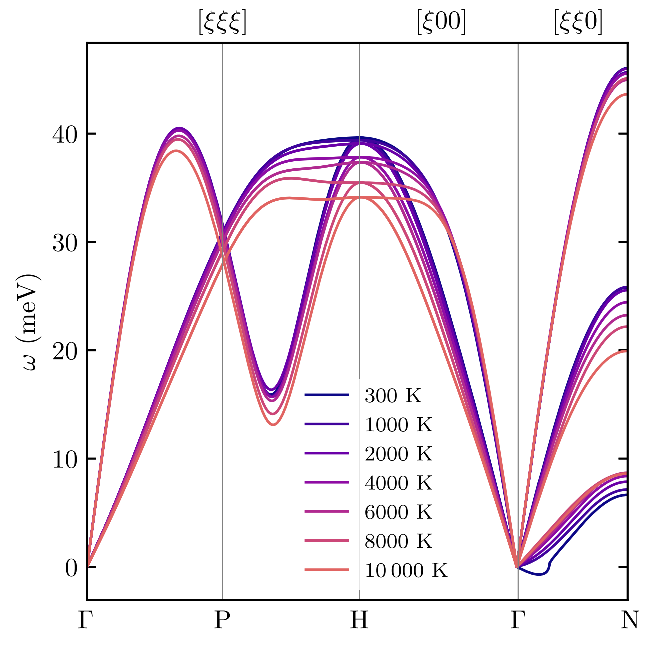

FIG. 5. Phonon spectrum of bcc-Au between 300 and 10 000 K along the $V = 77.69\ \mathrm{Bohr}^3/\mathrm{at}$ isochore (corresponding to $p_0 = 200$ GPa) computed using MLACS-TDEP.

temperature, the fcc phase transits toward the hcp one between 500 and 600 GPa. This results disagrees with experiments for which the fcc phase is stable up to 603 GPa. At intermediate temperature, we obtain a large fcc stability domain, from 0 to 600–800 GPa, consistent with the experimental observations made by isentropic compression [23,25]. Around 140–235 GPa and 6000–8000 K, we unveil the presence of a bcc small domain, also reported in shock experiments [21,22]. We demonstrate that this unexpected stabilization of the bcc phase with respect to other solid phases comes from anharmonic effects. We believe these NETI simulations accelerated by machine learning will be useful, not only to compute solid-solid transitions but also to determine solid-liquid transitions.

The authors thank Agnès Dewaele for fruitful discussions about the phase diagram of gold and experiments, and Gunnar Weck, Alexis Forestier and Paul Loubeyre for their helpful suggestions and comments.

[1] V. Cerantola, A. D. Rosa, Z. Konôpková, R. Torchio, E. Brambrink, A. Rack, U. Zastrau, and S. Pascarelli, J. Phys. Condens. Matter **33**, 274003 (2021).

[2] G. Shen and H. K. Mao, Rep. Prog. Phys. **80**, 016101 (2016).

[3] D. Batani, A. Balducci, D. Beretta, A. Bernardinello, T. Löwer, M. Koenig, A. Benuzzi, B. Faral, and T. Hall, Phys. Rev. B **61**, 9287 (2000).

[4] D. L. Heinz and R. Jeanloz, J. Appl. Phys. **55**, 885 (1984).

[5] P. M. Bell, J.-a. Xu, and H. K. Mao, in *Shock Waves in Condensed Matter*, edited by Y. M. Gupta (Springer US, Boston, MA, 1986), pp. 125–130, 10.1007/978-1-4613-2207-8_13.

[6] Y. Akahama, H. Kawamura, and A. K. Singh, J. Appl. Phys. **92**, 5892 (2002).

[7] J. C. Boettger, Phys. Rev. B **67**, 174107 (2003).

[8] T. Ishikawa, K. Kato, M. Nomura, N. Suzuki, H. Nagara, and K. Shimizu, Phys. Rev. B **88**, 214110 (2013).

[9] A. Dewaele, P. Loubeyre, and M. Mezouar, Phys. Rev. B **70**, 094112 (2004).

[10] A. Dewaele, M. Torrent, P. Loubeyre, and M. Mezouar, Phys. Rev. B **78**, 104102 (2008).

[11] K. Takemura and A. Dewaele, Phys. Rev. B **78**, 104119 (2008).

[12] O. L. Anderson, D. G. Isaak, and S. Yamamoto, J. Appl. Phys. **65**, 1534 (1989).

[13] C. W. Greeff and M. J. Graf, Phys. Rev. B **69**, 054107 (2004).

[14] P. Souvatzis, A. Delin, and O. Eriksson, Phys. Rev. B **73**, 054110 (2006).

[15] M. Yokoo, N. Kawai, K. G. Nakamura, K. I. Kondo, Y. Tange, and T. Tsuchiya, Phys. Rev. B **80**, 104114 (2009).

[16] P. A. Olsson, Comput. Mater. Sci. **99**, 361 (2015).

[17] L. Dubrovinsky, N. Dubrovinskaia, V. B. Prakapenka, and A. M. Abakumov, Nat. Commun. **3**, 1163 (2012).

[18] N. Dubrovinskaia, L. Dubrovinsky, N. A. Solopova, A. Abakumov, S. Turner, M. Hanfland, E. Bykova, M. Bykov, C. Prescher, V. B. Prakapenka, S. Petitgirard, I. Chuvashova, B. Gasharova, Y.-L. Mathis, P. Ershov, I. Snigireva, and A. Snigirev, Sci. Adv. **2**, e1600341 (2016).

[19] A. Dewaele, P. Loubeyre, F. Occelli, O. Marie, and M. Mezouar, Nat. Commun. **9**, 2913 (2018).

[20] W. Liu, X. Duan, S. Jiang, Z. Wang, L. Sun, H. Liu, W. Yang, H. Zhang, Q. Ye, P. Wang, Y. Li, L. Yi, and S. Dong, Phys. Plasmas **25**, 062707 (2018).

[21] R. Briggs, F. Coppari, M. G. Gorman, R. F. Smith, S. J. Tracy, A. L. Coleman, A. Fernandez-Pañella, M. Millot, J. H. Eggert, and D. E. Fratanduono, Phys. Rev. Lett. **123**, 045701 (2019).

[22] S. M. Sharma, S. J. Turneaure, J. M. Winey, Y. Li, P. Rigg, A. Schuman, N. Sinclair, Y. Toyoda, X. Wang, N. Weir, J. Zhang, and Y. M. Gupta, Phys. Rev. Lett. **123**, 045702 (2019).

[23] D. E. Fratanduono, M. Millot, D. G. Braun, S. J. Ali, A. Fernandez-Pañella, C. T. Seagle, J.-P. Davis, J. L. Brown, Y. Akahama, R. G. Kraus, M. C. Marshall, R. F. Smith, E. F. O'Bannon, J. M. McNaney, and J. H. Eggert, Science **372**, 1063 (2021).

[24] S. K. Han, R. F. Smith, D. Kim, J. K. Wicks, J. R. Rygg, A. Lazicki, J. H. Eggert, and T. S. Duffy, Phys. Rev. B **103**, 184109 (2021).

[25] F. Coppari, D. E. Fratanduono, M. Millot, R. G. Kraus, A. Lazicki, J. R. Rygg, R. F. Smith, and J. H. Eggert, Phys. Rev. B **106**, 134105 (2022).

[26] L. Dubrovinsky, N. Dubrovinskaia, W. A. Crichton, A. S. Mikhaylushkin, S. I. Simak, I. A. Abrikosov, J. S. de Almeida, R. Ahuja, W. Luo, and B. Johansson, Phys. Rev. Lett. **98**, 045503 (2007).

[27] G. Weck, V. Recoules, J.-A. Queyroux, F. Datchi, J. Bouchet, S. Ninet, G. Garbarino, M. Mezouar, and P. Loubeyre, Phys. Rev. B **101**, 014106 (2020).

[28] N. A. Smirnov, J. Phys. Condens. Matter **29**, 105402 (2017).

[29] R. Ahuja, S. Rekhi, and B. Johansson, Phys. Rev. B **63**, 212101 (2001).

[30] P. Söderlind, Phys. Rev. B **66**, 176201 (2002).

[31] Z. L. Liu, Y. P. Tao, X. L. Zhang, and L. C. Cai, Comput. Mater. Sci. **114**, 72 (2016).

[32] O. Hellman, I. A. Abrikosov, and S. I. Simak, Phys. Rev. B **84**, 180301(R) (2011).

[33] F. Bottin, J. Bieder, and J. Bouchet, Comput. Phys. Commun. **254**, 107301 (2020).

[34] See Supplemental Material at http://link.aps.org/supplemental/10.1103/PhysRevLett.131.206101 for more information about the TDEP method (see Sec. I), the MLACS procedure (see Sec. II), the validation of MLACS (see Sec. III), the NETI method (see Sec. IV), previous theoretical studies (see Sec. V), the ground state properties of Au (see Sec. VI), the effect of semicore electrons (see Sec. VII), the influence of **k**-points (see Sec. VIII), the NETI results (see Sec. IX), the DFPT and NETI phase diagrams (see Sec. X), the phonon spectrum of the fcc-Au phase (see Sec. XI) and the mechanical instability (see Sec. XII). This Supplemental Material includes Refs. [35–56].

[35] A. Thompson, L. Swiler, C. Trott, S. Foiles, and G. Tucker, J. Comput. Phys. **285**, 316 (2015).

[36] M. A. Wood and A. P. Thompson, J. Chem. Phys. **148**, 241721 (2018).

[37] M. A. Cusentino, M. A. Wood, and A. P. Thompson, J. Phys. Chem. A **124**, 5456 (2020).

[38] A. P. Thompson, H. M. Aktulga, R. Berger, D. S. Bolintineanu, W. M. Brown, P. S. Crozier, P. J. in 't Veld, A. Kohlmeyer, S. G. Moore, T. D. Nguyen, R. Shan, M. J. Stevens, J. Tranchida, C. Trott, and S. J. Plimpton, Comput. Phys. Commun. **271**, 108171 (2022).

[39] M. R. Shirts and J. D. Chodera, J. Chem. Phys. **129**, 124105 (2008).

[40] D. Frenkel and A. J. Ladd, J. Chem. Phys. **81**, 3188 (1984).

[41] C. Jarzynski, Phys. Rev. Lett. **78**, 2690 (1997).

[42] M. D. Koning, J. Chem. Phys. **122**, 104106 (2005).

[43] J. M. Polson, E. Trizac, S. Pronk, and D. Frenkel, J. Chem. Phys. **112**, 5339 (2000).

[44] G. Navascús and E. Velasco, J. Chem. Phys. **132**, 134106 (2010).

[45] R. W. Zwanzig, J. Chem. Phys. **22**, 1420 (1954).

[46] T. Lelièvre, M. Rousset, and G. Stoltz, *Free Energy Computations* (Imperial College Press, London, 2010), 10.1142/p579.

[47] J. P. Perdew, J. A. Chevary, S. H. Vosko, K. A. Jackson, M. R. Pederson, D. J. Singh, and C. Fiolhais, Phys. Rev. B **46**, 6671 (1992).

[48] J. P. Perdew, Phys. Rev. B **33**, 8822 (1986).

[49] J. P. Perdew, K. Burke, and M. Ernzerhof, Phys. Rev. Lett. **80**, 891 (1998).

[50] P. Vinet, J. Ferrante, J. H. Rose, and J. R. Smith, J. Geophys. Res. **92**, 9319 (1987).

[51] J. R. Neighbours and G. A. Alers, Phys. Rev. **111**, 707 (1958).

[52] A. Dewaele and P. Loubeyre, High Press. Res. **27**, 419 (2007).

[53] T. Sakai, T. Yagi, T. Irifune, H. Kadobayashi, N. Hirao, T. Kunimoto, H. Ohfuji, S. Kawaguchi-Imada, Y. Ohishi, S. Tateno *et al.*, High Press. Res. **38**, 107 (2018).

[54] J. W. Lynn, H. G. Smith, and R. M. Nicklow, Phys. Rev. B **8**, 3493 (1973).

[55] T. S. Duffy, G. Shen, D. L. Heinz, J. Shu, Y. Ma, H.-K. Mao, R. J. Hemley, and A. K. Singh, Phys. Rev. B **60**, 15063 (1999).

[56] F. Mouhat and F.-X. Coudert, Phys. Rev. B **90**, 224104 (2014).

[57] J. Bouchet and F. Bottin, Phys. Rev. B **92**, 174108 (2015).

[58] J. Bouchet and F. Bottin, Phys. Rev. B **95**, 054113 (2017).

[59] B. Dorado, F. Bottin, and J. Bouchet, Phys. Rev. B **95**, 104303 (2017).

[60] J. Bouchet, F. Bottin, V. Recoules, F. Remus, G. Morard, R. M. Bolis, and A. Benuzzi-Mounaix, Phys. Rev. B **99**, 094113 (2019).

[61] A. Castellano, F. Bottin, B. Dorado, and J. Bouchet, Phys. Rev. B **101**, 184111 (2020).

[62] S. Anzellini, F. Bottin, J. Bouchet, and A. Dewaele, Phys. Rev. B **102**, 184105 (2020).

[63] J. Bouchet, F. Bottin, D. Antonangeli, and G. Morard, J. Phys. Condens. Matter **34**, 344002 (2022).

[64] A. Castellano, F. Bottin, J. Bouchet, A. Levitt, and G. Stoltz, Phys. Rev. B **106**, L161110 (2022).

[65] D. Frenkel and B. Smit, *Understanding Molecular Simulation*, 2nd ed. (Academic Press, New York, 2002).

[66] M. Watanabe and W. P. Reinhardt, Phys. Rev. Lett. **65**, 3301 (1990).

[67] R. Freitas, M. Asta, and M. de Koning, Comput. Mater. Sci. **112**, 333 (2016).

[68] R. Paula Leite and M. de Koning, Comput. Mater. Sci. **159**, 316 (2019).

[69] I. A. Kruglov, A. Yanilkin, A. R. Oganov, and P. Korotaev, Phys. Rev. B **100**, 174104 (2019).

[70] P. E. Blöchl, Phys. Rev. B **50**, 17953 (1994).

[71] M. Torrent, F. Jollet, F. Bottin, G. Zérah, and X. Gonze, Comput. Mater. Sci. **42**, 337 (2008).

[72] The ABINIT code is a common project of the Catholic University of Louvain (Belgium), Corning Incorporated, CEA (France) and other Collaborators, http://www.abinit.org. (2022).

[73] X. Gonze *et al.*, Comput. Phys. Commun. **248**, 107042 (2020).

[74] J. P. Perdew and Y. Wang, Phys. Rev. B **45**, 13244 (1992).

[75] ATOMPAW is a general license public code developed at Wake Forest University. Some of its capabilities have been developed at the CEA, http://pwpaw.wfu.edu. (2022).

[76] S. M. Sharma, S. J. Turneaure, J. M. Winey, and Y. M. Gupta, Phys. Rev. Lett. **124**, 235701 (2020).

[77] P. Souvatzis, O. Eriksson, M. I. Katsnelson, and S. P. Rudin, Phys. Rev. Lett. **100**, 095901 (2008).

[78] A. Dewaele, V. Stutzmann, J. Bouchet, F. Bottin, F. Occelli, and M. Mezouar, Phys. Rev. B **91**, 134108 (2015).